Phase behavior of supported lipid bilayers: A systematic study by coarse-grained molecular dynamics simulations

Poursoroush, Asma; Sperotto, Maria Maddalena; Laradji, Mohamed

Published in:
Journal of Chemical Physics

Link to article, DOI:
10.1063/1.4981008

Publication date:
2017

Document Version
Publisher's PDF, also known as Version of record

Phase behavior of supported lipid bilayers: A systematic study by coarse-grained molecular dynamics simulations

Asma Poursoroush, Maria Maddalena Sperotto, and Mohamed Laradji

Citation: The Journal of Chemical Physics **146**, 154902 (2017); doi: 10.1063/1.4981008
View online: http://dx.doi.org/10.1063/1.4981008
View Table of Contents: http://aip.scitation.org/toc/jcp/146/15
Published by the American Institute of Physics

Phase behavior of supported lipid bilayers: A systematic study by coarse-grained molecular dynamics simulations

Asma Poursoroush,[1] Maria Maddalena Sperotto,[2] and Mohamed Laradji[1,a)]
[1]*Department of Physics and Materials Science, The University of Memphis, Memphis, Tennessee 38152, USA*
[2]*DTU Bioinformatics, Department of Bio and Health Informatics, Technical University of Denmark, DK-2800 Kongens Lyngby, Denmark*

(Received 14 January 2017; accepted 31 March 2017; published online 20 April 2017)

Solid-supported lipid bilayers are utilized by experimental scientists as models for biological membranes because of their stability. However, compared to free standing bilayers, their close proximity to the substrate may affect their phase behavior. As this is still poorly understood, and few computational studies have been performed on such systems thus far, here we present the results from a systematic study based on molecular dynamics simulations of an implicit-solvent model for solid-supported lipid bilayers with varying lipid-substrate interactions. The attractive interaction between the substrate and the lipid head groups that are closest to the substrate leads to an increased translocation of the lipids from the distal to the proximal bilayer-leaflet. This thereby leads to a transbilayer imbalance of the lipid density, with the lipid density of the proximal leaflet higher than that of the distal leaflet. Consequently, the order parameter of the proximal leaflet is found to be higher than that of the distal leaflet, the higher the strength of lipid interaction is, the stronger the effect. The proximal leaflet exhibits gel and fluid phases with an abrupt melting transition between the two phases. In contrast, below the melting temperature of the proximal leaflet, the distal leaflet is inhomogeneous with coexisting gel and fluid domains. The size of the fluid domains increases with increasing the strength of the lipid interaction. At low temperatures, the inhomogeneity of the distal leaflet is due to its reduced lipid density. *Published by AIP Publishing.* [http://dx.doi.org/10.1063/1.4981008]

I. INTRODUCTION

Many biological processes in the cell involve biological membranes,[1] which are complex multi-component systems composed of a double layer of lipids, the so-called lipid bilayer, where molecules such as proteins are embedded or attached. The molecular distribution in the two bilayer leaflets of biological membranes is asymmetric, which add to the complexity of such biosystems. Differently from a soft material such as a vulcanized rubber sheet, which is held together by covalent cross-links, biomembranes are soft biological materials, whose molecular components are individually held together by covalent bonds, but whose overall structure is maintained by weaker interactions, such as those due to hydrogen bonds and van der Waals forces. This guaranties that molecules are mobile within the membrane plane, hence allowing biochemical functions to occur. From the soft materials point of view, biomembranes are then viewed as two-dimensional fluids.[2]

In an aqueous solution, lipids extracted from biomembranes can spontaneously self-assemble into lipid bilayer systems. Reconstituted few-component systems, such as lamellar stacks, giant unilamellar/multilamellar vesicles, black lipid membranes, and supported lipid bilayers (SLBs), have thus been used as model biomimetic systems for understanding the physical and physico-chemical properties of biological membranes.[3] SLBs are systems made of lipid bilayers that are typically supported by SiO_2, glass, quartz, or mica substrates.[4] SLBs were introduced in the 1980s to investigate interactions between cells and lipid bilayers.[5,6] SLBs are prepared either by vesicle fusion,[7] Langmuir-Blodgett/Langmuir-Schaefer deposition,[8] or by the solvent assisted lipid bilayer method.[9] One of the advantages of using SLBs instead of giant unilamellar vesicles is that their preparation is relatively simpler and can be well characterized using surface-sensitive techniques, such as atomic force microscopy (AFM),[10–13] neutron reflection,[14] and epifluorescence microscopy,[7] which allow to study their in-plane morphology, thermodynamics, and their transbilayer asymmetry. Another advantage of using SLBs as models for biomembranes is that they can become asymmetric due to the interaction with the substrate.[15] However, because the aqueous film that separates the SLB from the substrate is thin (with a thickness typically between 0.5 and 2 nm), one would expect that the interaction with the substrate induces phase changes in the SLB that may not occur if the equivalent (composition wise) bilayer was not supported. Indeed, the physical properties of SLBs differ from those of free standing membranes or giant unilamellar vesicles.[15–18]

Several experimental studies, mostly based on AFM, were performed to investigate the phase behavior of SLBs[10,12,13,15,19–28] as a function of temperature, for different lipid species, substrates, and sample preparation conditions, as described in a recent review by Alessandrini and Facci.[29] Some of these experimental studies have shown that the two leaflets of the bilayer may undergo a gel-fluid phase change at two different temperatures, with the melting

a)Email: mlaradji@memphis.edu

temperature of the proximal leaflet, $T_p^{(m)}$, being slightly higher than that of the distal leaflet, $T_d^{(m)}$, where the proximal and distal leaflets refer to those nearest and farthest to the substrate, respectively.[12,13,22,24,25] In contrast, other studies have shown that both proximal and distal leaflets melt at the same temperature.[13,21,23,26–28,30] Regarding sample preparation effects, Seeger *et al.*[27] showed that the incubation temperature of the sample affects the phase behavior of 1-palmitoyl-2-oleoyl-*sn*-glycero-3-phosphoethanolamine (POPE) bilayers prepared by vesicles fusion on mica substrates. They found that the phase change of the distal and proximal leaflets is decoupled if the fusion is performed below the melting temperature of the vesicles. However, they found that the melting temperatures of the two leaflets are identical, if the fusion of the vesicles is performed above the melting temperature of the vesicles.[27] In a subsequent study, Seeger *et al.*[28] showed that, in the case of SLBs prepared from vesicles fusion on SiO_2 substrates, both leaflets undergo a phase change at the same temperature, regardless of the temperature at which the vesicle fusion is performed.

More recently, Ramkaran and Badia[10] used AFM to investigate the effects of the phase state and molecular density of the Langmuir monolayers on the melting behavior of mica-supported 1,2-dipalmytoyl-*sn*-3-phosphocoline (DPPC) and 1,2-dimyristoyl-*sn*-glycero-3-phosphocoline (DMPC) bilayers. The Langmuir monolayers were deposited on the substrate by the Langmuir-Blodgett and Langmuir-Schaefer technique. They found that the temperature at which the Langmuir-Blodgett and Langmuir-Schaefer lipid monolayers are transferred plays an important role on the melting behavior of each SLB's monolayer. In particular, they found that $T_p^{(m)}$ is higher than $T_d^{(m)}$, and that the difference $T_p^{(m)} - T_d^{(m)}$ increases with increasing the temperature at which the Langmuir films are transferred to the mica substrate. Furthermore, by analyzing the surface area fraction of the gel-phase as a function of temperature, they observed that the width of the transition region of both monolayers was broader than that of the corresponding unsupported systems (i.e., multilamellar lipid vesicles), and that the width related to the distal leaflet was broader than that of the proximal leaflet. It is noteworthy to add that they observed that, at low temperatures, the amount of defects (attributable to holes, depressions, and cracks) in the SLBs increases with increasing the temperature at which the Langmuir films are transferred.[10] As spontaneous transbilayer diffusion, the so-called flip-flop, of phospholipids is energetically unfavorable,[31–33] SLB defects such as pores might mediate the lipid lateral diffusion from the distal to the proximal leaflet and therefore contribute to the lipid density difference, hence an *imbalance* between the two leaflets. Regarding the pores hypothesis, this was recently considered by Marquardt *et al.*[34] to explain the huge difference in DPPC's flip-flop rate between DPPC large unilamellar vesicles and SLBs. In regard to the lipid density difference, molecular dynamics simulations on a coarse-grained model[35] have indeed shown that due to the effect of the substrate on the bilayer, there occurs an imbalance in the lipid density between the two leaflets, with the lipid density of the proximal leaflet being higher than that of the distal leaflet. However, experimental evidence of an imbalance in the lipid density of the two leaflets is lacking.[10,13,27] Whether the decoupling in the melting behaviors of the two leaflets results, as well, in different transport properties of the two leaflets was also the subject of several investigations. Several groups found the same lipid diffusivities in the distal and proximal leaflets[26,36–38] in the case of SLBs supported by glass substrates. In contrast, others found that, in the case of SLBs on mica, the diffusivity of the lipids in the proximal leaflet is lower than that of the distal leaflet.[26,39,40]

Several computational studies have been performed to investigate SLBs via molecular dynamics[35,41–50] and Monte Carlo simulations,[51] but the effect of solid substrates on the thermodynamic properties of lipid bilayers has not been investigated through numerical simulations. To our knowledge, no theoretical study has been performed to investigate the effect of solid substrates on the structural properties and phase behavior of lipid bilayers. A somewhat related theoretical study, by Loverde *et al.*,[52] of the phase behavior of two-component mixtures of oppositely charged particles that are adsorbed to a charge-neutral surface had shown that the surface leads to a rich phase behavior of the binary mixture.

In this article, we present a study which shows that, depending on the strength of the bilayer interaction, the substrate may lead to an asymmetric lipid distribution in the two leaflets, with a lipid density of the proximal leaflet that is higher than that of the distal leaflet. Furthermore, our study indicates that, although the melting transition temperature of each bilayer leaflet is only slightly affected by the strength of the bilayer interaction, this interaction affects the overall thermodynamics of the bilayer, as tracked from quantities such as internal energy and order parameter, which is mainly dominated by the proximal leaflet. In particular, we found that the translational order parameter of the proximal leaflet exhibits an abrupt transition for all considered values of the bilayer interaction, while that of the distal leaflet exhibits an abrupt transition only at low values of the interaction. However, for high values of the bilayer interaction, the order parameter of the distal leaflet only gradually increases with lowering temperature. At low temperatures and for all lipid-substrate interactions which we considered, the proximal leaflet is homogenous and in the gel phase. In contrast, the distal leaflet is inhomogeneous at low temperatures and consists of coexisting gel and fluid domains (although these do not necessarily constitute two-phase coexistence in the thermodynamic sense). The average size of the gel domains decreases with increasing the lipids interaction strength. The asymmetric behavior of the two leaflets is due to the translocation of lipids from the distal leaflet to the proximal leaflet, thereby leading to an imbalance in the lipid densities of the two leaflets.

In Section II, the model and method are presented. Results of the simulations are reported in Section III, and finally, a summary and conclusion of the study are presented in Section IV.

II. MODEL AND METHOD

To investigate the effect of solid substrates on the thermodynamics of lipid bilayers, we used a coarse-grained

implicit-solvent model that we previously adopted to study biomimetic membranes.[53,54] Apart from being computationally more advantageous, using an implicit-solvent model, rather than an explicit one, offers the advantage of controlling the strength of the substrate-lipid interaction. The strength depends on the thickness of the thin solvent film that is present between the lipid bilayer and the substrate. However, this thickness is not known and, in experiments, the presence of edges and pores may facilitate the transport of the solvent from this layer to the bulk. The transport process is not allowed in simulations, unless pores are artificially built in the model. Also, in implicit-solvent simulations, the thickness of the solvent film can vary arbitrarily, thereby affecting the strength of substrate-lipid interaction. Therefore, one would expect that the SLBs thermodynamics, as derived from an explicit-solvent model, depends on the thickness of the solvent film.

According to the considered model, lipid molecules are coarse-grained into short semi-flexible chains composed of three beads, one hydrophilic (h) followed by two hydrophobic (t). As the solvent, i.e., water, is not explicitly modeled, the self-assembly of the lipid molecules is achieved by making the interactions between the hydrophobic tail-beads of the lipids attractive. The potential energy of the lipid bilayer has three contributions as follows:

$$U\left(\{\mathbf{r}_i\}\right) = \sum_{i,j} U_0^{\alpha_i\alpha_j}\left(r_{ij}\right) + \sum_i{}' U_{\text{bond}}\left(r_{i,i+1}\right) + \sum_i{}'' U_{\text{bend}}\left(\mathbf{r}_{i-1}, \mathbf{r}_i, \mathbf{r}_{i+1}\right), \tag{1}$$

where $\mathbf{r}_i$ describes the position of bead i, and $r_{ij} = |\mathbf{r}_i - \mathbf{r}_j|$. For each type of bead i, $\alpha_i = h$ or t for a lipid head bead or a tail bead, respectively. In Eq. (1), $U_0^{\alpha_i\alpha_j}$ is a soft two-body potential between two beads i and j and is given by,

$$U_0^{\alpha\beta}(r) = \begin{cases} \left(U_{\max}^{\alpha\beta} - U_{\min}^{\alpha\beta}\right)\dfrac{(r_m - r)^2}{r_m^2} + U_{\min}^{\alpha\beta} & \text{if } r \le r_m \\ -2U_{\min}^{\alpha\beta}\dfrac{(r_c - r)^3}{(r_c - r_m)^3} + 3U_{\min}^{\alpha\beta}\dfrac{(r_c - r)^2}{(r_c - r_m)^2} & \text{if } r_m < r \le r_c \\ 0 & \text{if } r > r_c \end{cases}, \tag{2}$$

where $U_{\max}^{\alpha\beta} > 0$ for any pair (α, β). A negative value of $U_{\min}^{\alpha\beta}$ implies a short-range attraction between two beads of types α and β at intermediate distances. Here, we take $U_{\min}^{hh} = U_{\min}^{ht} = 0$ and $U_{\min}^{tt} < 0$ in order to produce stable self-assembled lipid bilayers.[54] $r_m \simeq 1$ nm and is used as the scale of length in this work. r_c is the cutoff of the potential energy set to $2r_m$. The interaction potential between lipid tail beads is shown in Fig. 1 of Ref. 53. We note that this implicit-solvent model predicts values of the bending modulus that are inline with experimental values. In particular, for the specific parameters used in the present study, the bending modulus of the bilayer in the fluid phase is $\kappa \simeq 34k_BT$. Furthermore, the value of lateral tension needed to produce lysis of the membrane is about $20\epsilon/r_m^2 \approx 20$ mN/m, in agreement for the lysis tension for giant unilamellar vesicles, which is about 10 mN/m.[55]

The interaction between a lipid bead and an element of area of the substrate, δa, is assumed to have the same form as that in Eq. (2), i.e.,

$$\delta U_0^{s\alpha}(r) = \begin{cases} \left[\left(U_{\max}^{s\alpha} - U_{\min}^{s\alpha}\right)\dfrac{(r_m - r)^2}{r_m^2} + U_{\min}^{s\alpha}\right]\zeta\delta a & \text{if } r \le r_m \\ \left[-2U_{\min}^{s\alpha}\dfrac{(r_c - r)^3}{(r_c - r_m)^3} + 3U_{\min}^{s\alpha}\dfrac{(r_c - r)^2}{(r_c - r_m)^2}\right]\zeta\delta a & \text{if } r_m < r \le r_c \\ 0 & \text{if } r > r_c \end{cases}, \tag{3}$$

where ζ is the beads number area density of the substrate. Here, we consider the case of a hydrophilic substrate that interacts attractively with the lipid head groups, but repulsively with the tail groups. We thus take $U_{\min}^{st} = 0$ and $U_{\min}^{sh} = -\mathcal{E} < 0$. The net potential energy between a lipid bead and the substrate obtained by integrating Eq. (3) is then given by

$$U_0^{s\alpha}(z) = \begin{cases} \pi\zeta U_{\min}^{s\alpha}\left(r_m^2 - z^2\right) + \dfrac{2\pi\zeta}{r_m^2}\left(U_{\max}^{s\alpha} - U_{\min}^{s\alpha}\right)\left[\dfrac{r_m}{3}(r_m - z)^3 - \dfrac{1}{4}(r_m - z)^4\right] \\ \quad + \dfrac{2\pi\zeta}{r_m^3}U_{\min}^{s\alpha}\left[\dfrac{2}{5}(r_c - r_m)^5 - \dfrac{7}{4}r_m(r_c - r_m)^4 + 2r_m^2(r_c - r_m)^3\right] & \text{if } 0 \le z \le r_m \\ \dfrac{2\pi\zeta}{r_m^3}U_{\min}^{s\alpha}\left[\dfrac{2}{5}(r_c - z)^5 - \dfrac{7}{4}r_m(r_c - z)^4 + 2r_m^2(r_c - z)^3\right] & \text{if } r_m \le z \le r_c \\ 0 & \text{if } z > r_c \end{cases}, \tag{4}$$

The strength of the substrate-bilayer interaction is defined as $\mathcal{E} = |U^{sh}_{\min}|$. The soft nature of the potential energy between lipid beads and the substrate allows for reasonably large time steps and therefore a systematic investigation over a wide range of temperature and $\mathcal{E}$. Furthermore, by selecting relatively large values of $U^{s\alpha}_{\max}$, beads are completely prevented from crossing the substrate surface, located at $z = 0$.

Consecutive beads that belong to the same lipid chain are bonded with each other through U_{bond} in Eq. (1) given by

$$U_{\text{bond}}(r) = \frac{k_{\text{bond}}}{2}(r - a_b)^2, \tag{5}$$

where k_{bond} is the bond stiffness coefficient and a_b is the preferred bond length. The last term in Eq. (1), U_{bend}, is a three-body potential, which provides stiffness to lipid molecules and is given by,

$$U_{\text{bend}}(\mathbf{r}_{i-1}, \mathbf{r}_i, \mathbf{r}_{i+1}) = \frac{k_{\text{bend}}}{2}\left(\cos\theta_0 - \frac{\mathbf{r}_{i,i-1} \cdot \mathbf{r}_{i,i+1}}{r_{i,i-1} r_{i,i+1}}\right)^2, \tag{6}$$

where k_{bend} is the bending stiffness coefficient and θ_0 is the preferred splay angle. Here, we take $\theta_0 = 180^{\text{o}}$. Values of the interaction parameters used in the model are

$$\begin{aligned}
U^{hh}_{\max} &= U^{ht}_{\max} = U^{st}_{\max} = 100\epsilon,\\
U^{tt}_{\max} &= U^{sh}_{\max} = 200\epsilon,\\
U^{hh}_{\min} &= U^{ht}_{\min} = U^{st}_{\min} = 0,\\
U^{sh}_{\min} &= -\mathcal{E},\\
k_{\text{bond}} &= 100\epsilon/r_m^2,\\
k_{\text{bend}} &= 100\epsilon,\\
r_c &= 2r_m,\\
a_b &= 0.7r_m,\\
\zeta &= 100 r_m^{-2}.
\end{aligned} \tag{7}$$

In the simulations, beads are moved using a molecular dynamics scheme with a Langevin thermostat[56]

$$\begin{aligned}
\dot{\mathbf{r}}_i(t) &= \mathbf{v}_i(t) \text{ and}\\
m\dot{\mathbf{v}}_i(t) &= -\nabla_i U(\{\mathbf{r}_i\}) - \Gamma \mathbf{v}_i(t) + \sigma \boldsymbol{\Xi}_i(t),
\end{aligned} \tag{8}$$

where m is the mass of a single bead (same for all beads), Γ is a bead's friction coefficient, and $\sigma\boldsymbol{\Xi}_i(t)$ is a random force due to the heat bath, with the random vector, $\boldsymbol{\Xi}_i(t)$, obeying

$$\langle \boldsymbol{\Xi}_i(t) \rangle = 0, \tag{9}$$

$$\langle \Xi^{(\mu)}_i(t)\, \Xi^{(\nu)}_j(t') \rangle = \delta_{\mu\nu}\delta_{ij}\delta(t - t'), \tag{10}$$

with $\mu, \nu = x, y,$ or z. To achieve thermal equilibrium, Γ and σ are inter-related through the fluctuation-dissipation theorem leading to $\Gamma = \sigma^2/2k_{\text{B}}T$.

The simulations are performed in the $NVT\Sigma$ ensemble, where N is the total number of beads in the system, $V = L_x L_y L_z$ is the system volume, and Σ is the lateral tension of the bilayer. Changes in the lateral size of the system are performed using the Metropolis Monte Carlo approach[57] with an effective Hamiltonian,

$$\mathcal{H} = U(\{\mathbf{r}_i\}) + \Sigma A_p - N k_B T \ln\left(L_z A_p / r_m^3\right), \tag{11}$$

where $A_p = L_x L_y$ is the projected area of the bilayer with the constraint $L_x = L_y$ and the bilayer is parallel to the xy-plane. We note that unlike a Langmuir-Blodget film at a water/air interface or a closed vesicle, the control or measurement of the lateral tension of a supported lipid bilayer is very challenging. Hence, we opted for simulations of tensionless SLBs.

During a single time step, the equations of motion of all beads are integrated using the velocity-Verlet algorithm[58] with $\Gamma = \sqrt{6}m/\tau$, where the model's time scale $\tau = r_m(m/\epsilon)^{1/2}$ with r_m and ϵ being used here as scales for length and energy. Then, an attempted new linear size of the system along the xy-plane $L'_x = L_x + \Lambda$ is selected with Λ being a small random deviation in length in the interval $(-0.1r_m, 0.1r_m)$. Attempted new bead positions are rescaled to $x'_i = x_i L'_x/L_x$, $y'_i = y_i L'_x/L_x$, and $z'_i = z_i (L_x/L'_x)^2$. The acceptance or rejection of this attempt is performed using the standard Metropolis criterion with the effective Hamiltonian in Eq. (11). All simulations are performed with periodic boundary conditions along the xy-plane on bilayers composed of 3000 lipid chains. We have used a time step $\Delta t = 0.01\tau$.

III. RESULTS

The phase behavior of the supported bilayer is investigated by analyzing the internal energy of the bilayer, E, and the translational order parameter, Ψ, as a function of temperature and strength of the substrate-bilayer interaction. Ψ is defined as

$$\Psi_\alpha = \left\langle \frac{1}{N_\alpha} \sum_{i=1}^{N_\alpha} \delta_{n_i,6} \right\rangle, \tag{12}$$

where $\delta_{k,l}$ is the Kronecker delta, and $\alpha = p$ or d for the proximal or distal leaflet, respectively. N_α is the number of lipid chains in leaflet α and n_i is the number of nearest neighbor chains of chain i, along the xy-plane. Projected centers of mass of the chains on the xy-plane are used and the number of nearest neighbors is determined using a Voronoi construction. A lipid is considered in the gel phase when the number of its nearest neighbors is equal to six.

Before presenting the results for the internal energy and chain order parameter of the SLBs, snapshots of equilibrium configurations of the proximal and distal leaflets at different temperatures, and for different values of the substrate-bilayer interaction strength, $\mathcal{E}$, are shown in Fig. 1, where lipid chains with high values of the order parameter are shown in blue, and chains with low values of the order parameter are shown in red. The labels p and d stand for the proximal and distal leaflet, respectively. The behaviors of the two leaflets in the absence of a substrate ($\mathcal{E} = 0$) are identical in average, as expected, with high order at low temperatures and low order at high temperature (hence only one leaflet is shown). The behaviors of the two leaflets for finite values of $\mathcal{E} > 0$ are clearly different, with the proximal leaflet exhibiting higher order than the distal leaflet at all temperatures. This figure also shows that the proximal leaflet for $\mathcal{E} > 0$ is mainly homogeneous, with a behavior that is very similar to that in the absence of a substrate. In contrast, the distal leaflet is inhomogeneous at low temperatures, with clear gel and fluid domains. Furthermore, Fig. 1 suggests that the average size of the fluid domains increases with increasing $\mathcal{E}$ at a given temperature below the melting transition of the proximal leaflet.

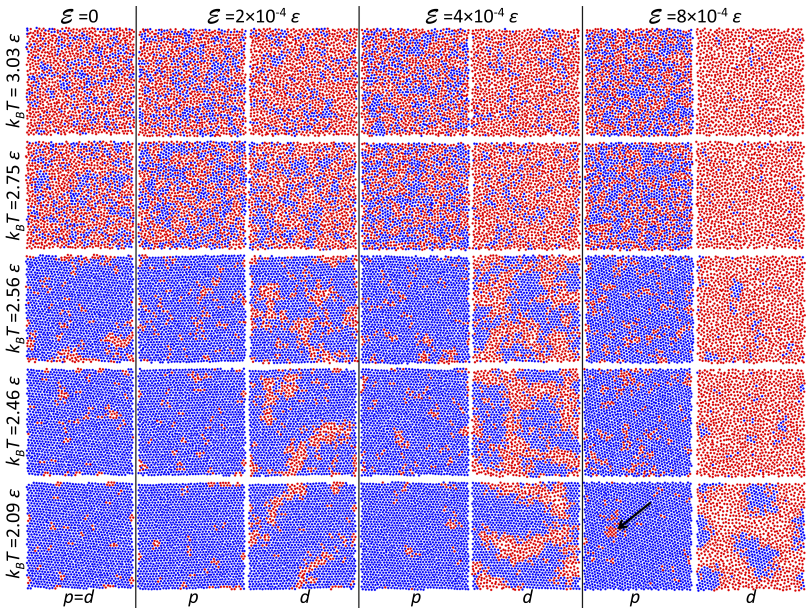

FIG. 1. Equilibrium snapshots of bilayers composed of 3000 lipid chains for different values of the bilayer interaction strength, $\mathcal{E} = 0$, $2 \times 10^{-4}\epsilon$, $4 \times 10^{-4}\epsilon$, and $8 \times 10^{-4}\epsilon$. Columns p and d correspond to the proximal and distal leaflets of the bilayer, respectively. Note that in the case of $\mathcal{E} = 0$, the proximal and distal leaflets are similar, and therefore only one leaflet is shown. Snapshots from the bottom to top correspond to temperatures ranging between $2.09\epsilon/k_B$ and $3.03\epsilon/k_B$. Blue beads correspond to the centers of mass of chains with six nearest neighbors (i.e., lipids in the gel state) and red beads correspond to the center of mass of chains with a number of nearest neighbors that is different from six (i.e., lipid chains in the fluid phase). The arrow in snapshot p at $k_BT = 2.09\epsilon$ for $\mathcal{E} = 8 \times 10^{-3}\epsilon$ indicates a region where the lipid chains are locally ordered in a square lattice.

The average area fraction of the fluid domains is shown in Fig. 2 as a function of temperature, and for different values of the adhesion strength, $\mathcal{E}$. This figure indicates that the area of the fluid domains decreases with decreasing temperature for both leaflets regardless of the value of $\mathcal{E}$. It also shows that at a given T and $\mathcal{E}$, the relative amount of fluid phase is larger in the distal leaflet than the proximal leaflet. Furthermore, for a given temperature, this figure shows that the amount of fluid phase in the distal leaflet increases with increasing $\mathcal{E}$, in agreement with what the snapshots of Fig. 1 suggest.

The average size of both gel and fluid domains is calculated from the cluster size distribution and is shown in Fig. 3 as a function of $\mathcal{E}$ at $k_BT = 2\epsilon$. This figure shows again that the size of the fluid domains increases with increasing $\mathcal{E}$, in agreement with Fig. 1. From the snapshots in Fig. 1, it appears that below the melting point and for low values of $\mathcal{E}$, the fluid domains in the distal leaflet are elongated (e.g., see snapshot d for $\mathcal{E} = 2 \times 10^{-4}\epsilon$ at $k_BT = 2.09\epsilon$). In contrast, at high values of $\mathcal{E}$, the gel domains are compact (e.g., see snapshot d for $\mathcal{E} = 8 \times 10^{-4}\epsilon$ at $k_BT = 2.09\epsilon$). In order to quantify this, we calculated a distortion parameter defined as L/R, where L and R are the average interfacial length and linear domain size, respectively. This is depicted in the inset of Fig. 3, which shows that for $\mathcal{E} = 2 \times 10^{-4}\epsilon$, $L/R \simeq 8$ for the fluid domains. In contrast, at $\mathcal{E} = 8 \times 10^{-4}\epsilon$, $L/R \simeq 3.5$ for the gel domains, which implies that while the fluid domains tend to be elongated, the gel domains tend to be compact, in accord with what the low temperature snapshots of Fig. 1 suggest.

The internal energy of the SLBs, per lipid chain, vs temperature, and for different values of $\mathcal{E}$ ranging between 0 and $8 \times 10^{-4}\epsilon$ is shown in Fig. 4. The melting temperature, T_m, determined from the internal energy, is shown as a function of $\mathcal{E}$ in Fig. 5. This figure indicates that for relatively low values of substrate-bilayer interaction strength, $\mathcal{E} \lesssim 2 \times 10^{-4}\epsilon$, the melting temperature remains unaffected but further decreases with the increase of $\mathcal{E}$. However, it is noted that the change in the melting transition is relatively weak and does not exceed 1.5%. Fig. 4 also shows that the melting transition is weak for

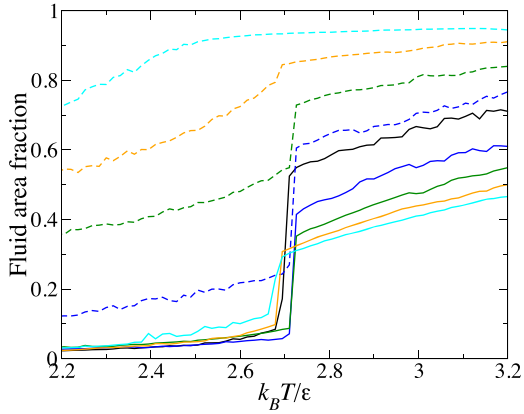

FIG. 2. Fluid phase area fraction vs temperature for the proximal leaflet (solid curves) and distal leaflet (dashed curves). Solid curves from top to bottom, at $k_BT = 3\epsilon$, correspond to $\mathcal{E} = 0$ (black), $2 \times 10^{-4}\epsilon$ (blue), $4 \times 10^{-4}\epsilon$ (green), $6 \times 10^{-4}\epsilon$ (orange), and $8 \times 10^{-4}\epsilon$ (cyan), respectively. Dashed curves from bottom to top at at $k_BT = 3\epsilon$ correspond to $\mathcal{E} = 2 \times 10^{-4}\epsilon$ (blue), $4 \times 10^{-4}\epsilon$ (green), $6 \times 10^{-4}\epsilon$ (orange), and $8 \times 10^{-4}\epsilon$ (cyan), respectively.

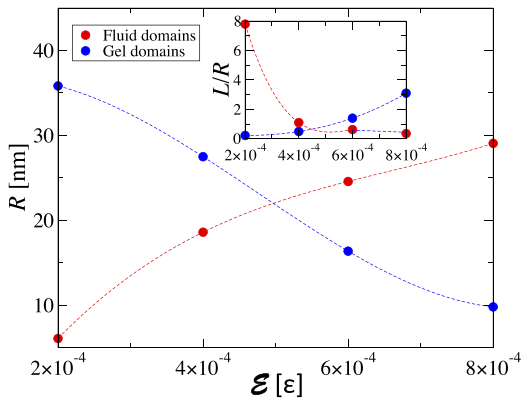

FIG. 3. The average size of fluid domains (blue markers) and gel domains (red markers) vs the adhesion strength, $\mathcal{E}$, at $k_BT = 2\epsilon$. Inset shows a measure of domain elongation, L/R, where L is the average net domain interfacial length and R is the average domain size, as a function of $\mathcal{E}$. The solid lines in both figure and inset are simply guides to the eye.

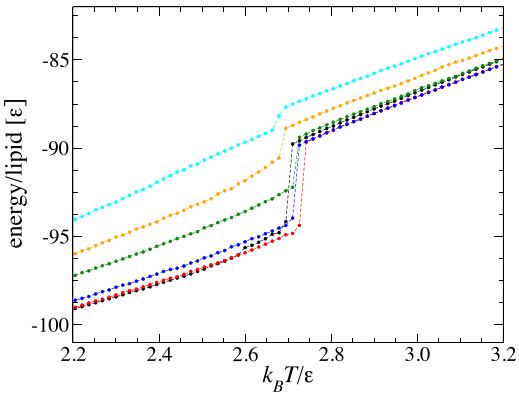

FIG. 4. Internal energy per lipid vs function of temperature. Curves from bottom to top (at $k_BT = 2.2\epsilon$) correspond to $\mathcal{E} = 0$ (black), $1\times10^{-4}\epsilon$ (red), $2\times10^{-4}\epsilon$ (blue), $4\times10^{-4}\epsilon$ (green), $6\times10^{-4}\epsilon$ (orange), and $8\times10^{-4}\epsilon$ (cyan), respectively.

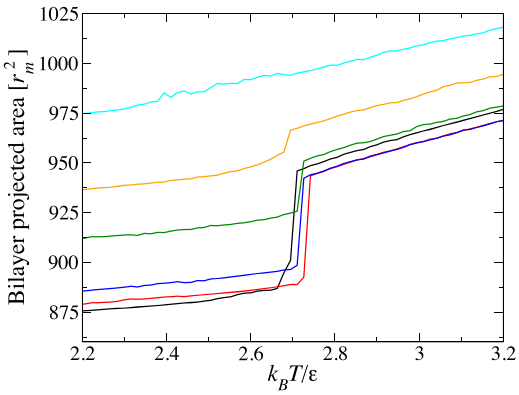

FIG. 6. Bilayer projected area vs temperature for different values of $\mathcal{E}$. Color coding of the curves is the same as in Fig. 4. Curves from bottom to top, at $k_BT = 2.2\epsilon$, correspond to $\mathcal{E} = 0$ (black), $1\times10^{-4}\epsilon$ (red), $2\times10^{-4}\epsilon$ (blue), $4\times10^{-4}\epsilon$ (green), $6\times10^{-4}\epsilon$ (orange), and $8\times10^{-4}\epsilon$ (cyan), respectively.

the highest considered substrate-bilayer interaction strength, $\mathcal{E} = 8\times10^{-4}\epsilon$.

The bilayer's projected area, $\mathcal{A}$, vs temperature is shown in Fig. 6 for different values of the substrate-bilayer interaction strength, $\mathcal{E}$. It can be seen that, except for $\mathcal{E} = 8\times10^{-4}\epsilon$, the bilayer undergoes compression with decreasing temperature, and that a sharp change in the projected area occurs at the same melting temperature as seen in Fig. 4. Similarly to what happens to the internal energy, the change in $\mathcal{A}$ at the melting temperature decreases with increasing $\mathcal{E}$, implying a weakening of the transition, and completely disappears at $\mathcal{E} = 8\times10^{-4}\epsilon$. Below the melting temperature, $\mathcal{A}$ increases with increasing $\mathcal{E}$. However, above the melting transition, $\mathcal{A}$ changes non-monotonically with $\mathcal{E}$.

To understand what happens to the two leaflets of the SLB, the lipid average densities of the proximal leaflet (solid lines) and distal leaflet (dashed lines) are shown in Fig. 7 as a function of temperature, and for different values of $\mathcal{E}$. For all temperatures, the lipid density of the proximal leaflet increases with increasing $\mathcal{E}$, whereas that of the distal leaflet decreases with increasing $\mathcal{E}$. From Figs. 6 and 7, we can infer that two competing effects are in play here as follows: (1) A decrease in the area per lipid in the proximal leaflet with increasing $\mathcal{E}$, which tends to decrease the bilayers area and (2) a transbilayer migration of the lipids from the distal to the proximal leaflet,

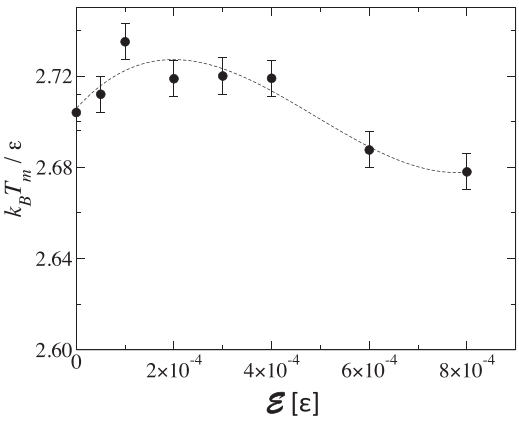

FIG. 5. Melting point vs the substrate-bilayer interaction strength, $\mathcal{E}$. The dashed solid line is just a guide to the eye.

which tends to increase the bilayer's area. The increase of $\mathcal{A}$ with increasing $\mathcal{E}$, at a given temperature, implies that the lipids transbilayer migration from the distal to proximal leaflet is stronger than the effect due to the increase in the lipid density of the proximal leaflet. A consequence of the decrease in the lipid density of the distal leaflet is that the number of lipids present in it becomes too small to have a monolayer where all lipids are in the gel phase at low temperatures. As a result, and as illustrated by the configurations of the distal leaflet below the melting point in Fig. 1, for $\mathcal{E} > 0$, only a fraction of the lipids undergo a phase transition to the gel phase, while others remain in the fluid phase, such as the leaflet is completely covered by lipids. This is in agreement with the recent experimental findings of Ramkaran and Badia[10] (see low temperature AFM images in Figs. 2 and 3 of Ref. 10).

Fig. 8 shows the order parameters of the proximal and distal leaflets (solid and dashed lines, respectively) as a function of temperature, and for different values of $\mathcal{E}$, as calculated using Eq. (12). It can be seen that for any value of $\mathcal{E} > 0$, the order parameter of the proximal leaflet is always higher than that of the distal leaflet. This is expected since the lipid density of the proximal leaflet is always higher than that of the

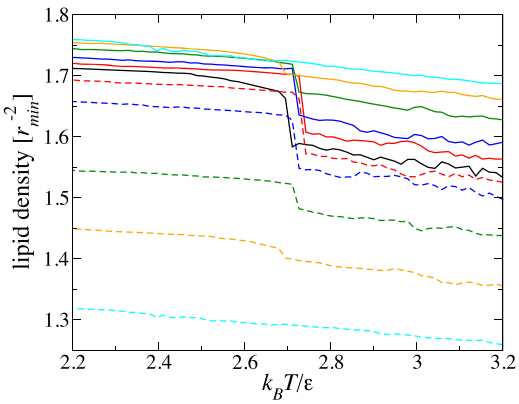

FIG. 7. Lipid density vs temperature for the proximal leaflet (solid curves) and distal leaflet (dashed curves). Solid curves from bottom to top, at $k_BT = 3\epsilon$, correspond to $\mathcal{E} = 0$ (black), $1\times10^{-4}\epsilon$ (red), $2\times10^{-4}\epsilon$ (blue), $4\times10^{-4}\epsilon$ (green), $6\times10^{-4}\epsilon$ (orange), and $8\times10^{-4}\epsilon$ (cyan), respectively. Dashed curves from top to bottom at $k_BT = 3\epsilon$ correspond to $\mathcal{E} = 1\times10^{-4}\epsilon$ (red), $2\times10^{-4}\epsilon$ (blue), $4\times10^{-4}\epsilon$ (green), $6\times10^{-4}\epsilon$ (orange), and $8\times10^{-4}\epsilon$ (cyan), respectively.

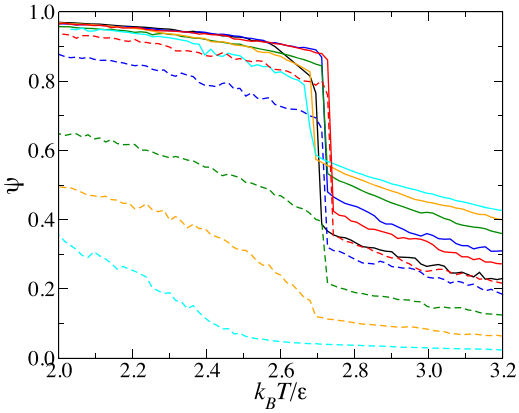

FIG. 8. Translation order parameter vs temperature for the proximal leaflet (solid curves) and distal leaflet (dashed curves). Solid curves from bottom to top at $k_BT = 3\epsilon$ correspond to $\mathcal{E} = 0$ (black), $1\times10^{-4}\epsilon$ (red), $2\times10^{-4}\epsilon$ (blue), $4\times10^{-4}\epsilon$ (green), $6\times10^{-4}\epsilon$ (orange), and $8\times10^{-4}\epsilon$ (cyan), respectively. Dashed curves from top to bottom at $k_BT = 3\epsilon$ correspond $1\times10^{-4}\epsilon$ (red), $2\times10^{-4}\epsilon$ (blue), $4\times10^{-4}\epsilon$ (green), $6\times10^{-4}\epsilon$ (orange), and $8\times10^{-4}\epsilon$ (cyan), respectively.

distal leaflet for $\mathcal{E} > 0$, cf. Fig. 7. Fig. 8 also shows that, at low temperatures, the order parameter of the proximal leaflet is not very sensitive to the bilayer-substrate interaction, as it shows a slight decrease as $\mathcal{E}$, despite the increase in the lipid density of the proximal leaflet with increasing $\mathcal{E}$, cf. Fig. 7. We attribute this to defects resulting from the lipids lateral rearrangement in the proximal leaflet. In fact, as suggested by the snapshot in Fig. 1, in column p ($\mathcal{E} = 8\times10^{-4}\epsilon$), and at $k_BT = 2.09\epsilon$, some chains are locally ordered in a square lattice instead of a triangular lattice, which contributes to a decrease in the order parameter.

Fig. 8 shows that for $T > T_m$, the order parameter of the proximal leaflet increases with increasing $\mathcal{E}$. This is inline with what the snapshots of the proximal leaflets clearly indicate (see columns p in Fig. 1) for $T > T_m$, namely that the number of lipids in the gel state (blue chains) increases with increasing $\mathcal{E}$. This is due to a decrease in the amount of chains conformations as a result of increase in the lipid density of the proximal leaflet with increasing the attraction between the substrate and the lipid head groups, cf. Fig. 7. In contrast, for both $T < T_m$ and $T > T_m$, the order parameter of the distal leaflet, Ψ, decreases with increasing $\mathcal{E}$. Again, this behavior correlates very well with what the snapshots in Fig. 1 indicate, namely that the number of lipids in the fluid state (red chains) increases with increasing $\mathcal{E}$.

Fig. 8 also illustrates that for $\mathcal{E} \le 6\times10^{-4}\epsilon$, both order parameters of the proximal and distal leaflets exhibit a transition at the same temperature. For $\mathcal{E} = 8\times10^{-4}\epsilon$, the order parameter of the proximal leaflet exhibits a clear transition at $T_m \approx 2.68\epsilon/k_B$. However, this is not the case for the order parameter of the distal leaflet, which gradually increases without showing an abrupt change. This is consistent with what can be seen from the snapshots of the distal leaflet for $\mathcal{E} = 8\times10^{-4}\epsilon$. These snapshots suggest that the distal leaflet is fairly homogeneous at $k_BT = 2.46\epsilon$, but at temperatures well below the melting temperature of the proximal leaflet, gel domains form.

To validate the results above, we propose a simple mean field theory based on the Bragg-Williams approximation of two apposed lattices where each site can be either in a singly-degenerate gel state or a multiply degenerate fluid state.[59–61] According to this theory, the numbers of lipids in the distal leaflet, N_d, and proximal leaflet, N_p, are not constant, but the total number of lipids in the bilayer, $N = N_d + N_p$, is constant. The free energy per lipid of this model can then be written as

$$\begin{aligned}\frac{\Delta F}{N} &= \frac{\chi}{2}\left[x\phi_d(1-\phi_d)+(1-x)\phi_p(1-\phi_p)\right]-\epsilon_{ad}(1-x)\\ &+\epsilon_f\left[(1-x)(1-\phi_p)+x(1-\phi_d)\right]+\epsilon_g\left[(1-x)\phi_p+x\phi_d\right]\\ &+\epsilon_{cpl}x(1-x)\left[\phi_p\left(1-\phi_d\right)+\left(1-\phi_p\right)\phi_d\right]\\ &+k_BT\left\{(1-x)\left[\phi_p\ln\phi_p+(1-\phi_p)\ln\left(\frac{1-\phi_p}{D_f}\right)\right]\right.\\ &\left.+x\left[\phi_d\ln\phi_d+(1-\phi_d)\ln\left(\frac{1-\phi_d}{D_f}\right)\right]\right\},\end{aligned} \tag{13}$$

where ϕ_d and ϕ_p are the fractions of lipids in the fluid state in the distal and proximal leaflets, respectively, and $x = N_d/(N_d + N_p)$ is the fraction of lipids in the distal leaflet. In Eq. (13), χ represents the strength of interaction between lipids in the same leaflet and ϵ_{cpl} is the strength of interaction between lipids belonging to apposing leaflets. ϵ_{ad} is the adhesion energy, which is negative. ϵ_g and ϵ_f are the intramolecular energies of a lipid in the gel and fluid states, respectively. D_f in the degeneracy of a lipid in the fluid state. We assume that the degeneracy of a lipid in the gel phase is $D_g = 1$.

The model assumes that the lateral area of a lipid in the fluid state, a_f, is higher than that in the gel state, a_g. Since the areas of the distal and proximal leaflets are equal, x is related to ϕ_d and ϕ_p through

$$x = \frac{(1-\tilde{a}_f)\phi_p + \tilde{a}_f}{(1-\tilde{a}_f)(\phi_p+\phi_d)+2\tilde{a}_f}, \tag{14}$$

where $\tilde{a}_f = a_f/a_g$.

The free energy, in Eq. (13), is then minimized with respect to ϕ_d, ϕ_p, and x for different temperatures and different values of the adhesion strength, ϵ_{ad}. We considered the case where $\epsilon_{cpl} = 0.3\chi$, $\epsilon_g = 0$, $\epsilon_f = 2\chi$, $D_f = 1000$, and $\tilde{a}_f = 1.65$. We note that changing these values only affects the details, but not the overall behavior of the calculated functions.

The area fraction of the lipids in the fluid phase defined as $(1-\phi_d)\tilde{a}_f/(\phi_d + (1-\phi_d)\tilde{a}_f)$ is shown in Fig. 9 as a function of reduced temperature, k_BT/χ for different values of the adhesion strength ranging between 0 and 0.4χ. Despite the simplicity of the mean field description above, Fig. 9 is in good qualitative agreement with our simulation results, particularly with Fig. 2, namely that the area fraction of lipids in the fluid state is higher in the distal leaflet than the proximal leaflet. Furthermore, the melting transitions of the two leaflets occur at the same temperature for low values of adhesion strength. However, at high adhesion strength, a decoupling between the melting transitions of the two leaflets is observed. The theory also predicts that for low values of adhesion strength, the melting transition increases with increasing ϵ_{ad} for low adhesion strength, in qualitative agreement with our simulate results.

The recent study of Ramkaran and Badia[10] showed that the phase behavior of both DPPC and DMPC SLBs on mica

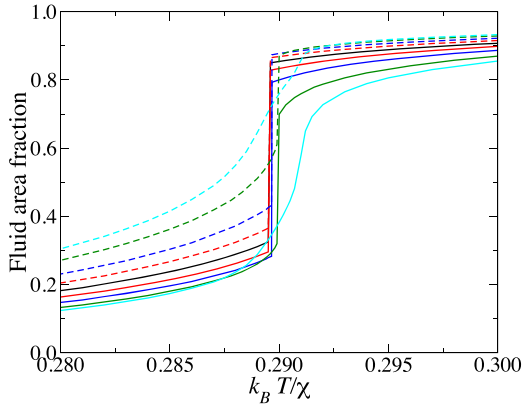

FIG. 9. Area fraction of lipids in the fluid state as obtained from the minimization of the free energy in Eq. (13). Solid and dashed lines correspond to the proximal and distal leaflets, respectively. Solid curves from top to bottom at $k_BT/\chi = 0.28$ correspond to $\epsilon_{ad}/\chi = 0$ (black), 0.10 (red), 0.20 (blue), 0.32 (green), and 0.40 (cyan), respectively. Dashed curves from bottom to top at $k_BT/\chi = 0.28$ correspond to $\epsilon_{ad}/\chi = 0$ (black), 0.10 (red), 0.20 (blue), 0.32 (green), and 0.40 (cyan), respectively.

depends on the temperature, T_{Lang}, at which the Langmuir monolayers are transferred to the substrate. For high T_{Lang}, the formed SLB exhibits pore-like defects at low temperatures, and the order parameter of the distal leaflet is much lower than that of the proximal leaflet. In contrast, for low T_{Lang}, i.e., when the transferred Langmuir monolayers are in the condensed phase, the amount of pores in the SLB at low temperatures is low, and the difference between the order parameters of the two leaflets is relatively low. We argue that the pore-like structures mediate lipid transfer from the distal leaflet to the proximal leaflet via their lateral diffusion and therefore allow for a greater density imbalance between the two leaflets leading to a weaker phase change of the distal leaflet than the proximal leaflet. In contrast, when the pores are almost absent, which is the case for low T_{Lang}, an increase in the lipid density of the proximal leaflet should be mainly due to induced lipid flip-flop. Hence, a reduced density imbalance in this case is expected, due to the low rate of lipid flip-flops, leading to a smaller difference in the order parameter of the two leaflets. The behavior of the order parameter in our simulation at $\mathcal{E} = 8\times10^{-4}\epsilon$ bares strong similarity with that of DMPC at $T_{Lang} = 25\,^{\circ}$C in Ref. 10.

In order to substantiate our argument, we performed a simulation for $\mathcal{E} = 8\times10^{-4}\epsilon$, while suppressing the possibility of lipid flip-flop. This is done by making the interaction between tail beads of one leaflet and head beads of the apposing leaflet (as described by Eq. (3)), more repulsive, namely, by choosing $U^{ht}_{\max} = 400\epsilon$ when h and t belong to apposing leaflets, and $U^{ht}_{\max} = 100\epsilon$ when head and tail beads belong to the same leaflet. Fig. 10 shows that, in this case, the two leaflets behave almost identically despite the strong attractive interaction between the head groups of the proximal leaflet and the substrate. This implies that the strong difference in the order parameters of the distal and proximal leaflets for $\mathcal{E} > 0$ is primarily due to an imbalance in the lipid density of the two leaflets, which is caused by the substrate-driven transbilayer migration from the distal to proximal leaflet.

We found that the effect caused by the substrate manifests, too, in the behavior of the lipid diffusion coefficients of the distal leaflet, D_d, and proximal leaflet, D_p. These were

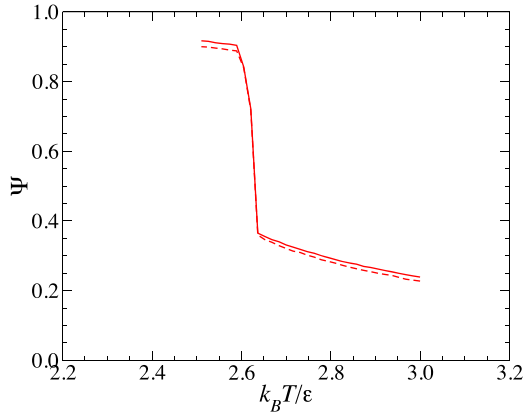

FIG. 10. Order parameter vs temperature for the case of $\mathcal{E} = 8\times10^{-4}\epsilon$ without lipid flip-flop, i.e., for equal densities of the proximal and distal leaflets. The solid and dashed lines correspond to the proximal and distal leaflets, respectively.

calculated using Einstein's relation,

$$D_\alpha = \frac{1}{4N_\alpha t}\left\langle \sum_{i=1}^{N_\alpha} |\mathbf{x}^{(cm)}_{\alpha,i}(t_0+t) - \mathbf{x}^{(cm)}_{\alpha,i}(t_0)|^2 \right\rangle, \qquad (15)$$

where $\mathbf{x}^{(cm)}_{\alpha,i} = (x^{(cm)}_{\alpha,i}, y^{(cm)}_{\alpha,i})$ are the in-plane coordinates of the center of mass of lipid j in leaflet α, and N_α is the number of lipids in that leaflet. The brackets in Eq. (15) indicate an average over initial times, t_0.

D_d and D_p vs temperature are shown in Fig. 11 for different values of the substrate-bilayer interaction strength. Note

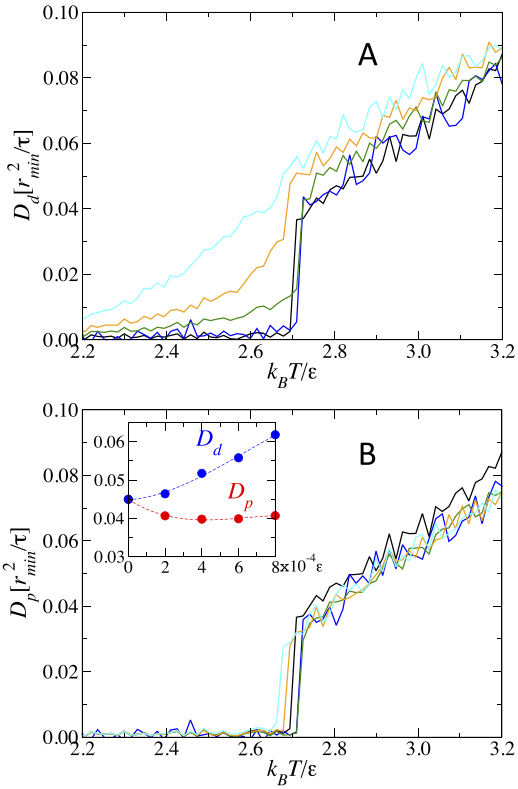

FIG. 11. Lipids diffusion coefficient of the distal leaflet (a) and proximal leaflet (b). Black, blue, green, orange, and cyan curves correspond to $\mathcal{E} = 0$, $2\times10^{-4}\epsilon$, $4\times10^{-4}\epsilon$, $6\times10^{-4}\epsilon$, and $8\times10^{-4}\epsilon$, respectively. The inset in (b) shows the diffusion coefficient vs $\mathcal{E}$ at $k_BT = 2.8\epsilon$ for the proximal leaflet (blue markers) and distal leaflet (red markers).

that lipids that underwent flip-flop were excluded from the diffusion calculation. As seen in Fig. 11, D_d and D_p increase with increasing temperature, as expected, and for $\mathcal{E} \lesssim 6 \times 10^{-4}\epsilon$, both D_d and D_p exhibit an abrupt change at the melting transition. An abrupt change in diffusivity was observed in DPPC bilayers both experimentally[62] and by molecular dynamics simulations.[63] However, for $\mathcal{E} = 8 \times 10^{-4}\epsilon$, while D_p abruptly changes at the melting temperature of the proximal leaflet, the distal leaflet exhibits a continuous change in a way similar to the order parameter of the distal leaflet. Furthermore, whereas the diffusivity of the lipids in the proximal leaflet is almost zero for all values of $\mathcal{E}$, the diffusivity of the lipids in the distal leaflet is finite at low temperatures for $\mathcal{E} > 2 \times 10^{-4}\epsilon$. This is due to the fact that a fraction of the lipids of the distal leaflet is in the fluid phase at low temperatures. The inset of Fig. 11(b) also shows that lipids in the distal leaflet have higher diffusion than those in the proximal leaflet, $D_d > D_p$ for $\mathcal{E} > 0$; it also shows that at temperatures above the melting temperature of the unsupported bilayer, D_d slightly increases with increasing $\mathcal{E}$, while D_p is almost insensitive to $\mathcal{E}$. Therefore, the difference between the diffusivity of the distal and proximal leaflet increases with increasing $\mathcal{E}$, with a largest change (~50%) occurring at $\mathcal{E} = 8 \times 10^{-4}\epsilon$. These results are in agreement with several earlier experimental findings.[26,36–38]

IV. SUMMARY AND CONCLUSION

In this article, we report the results of a systematic molecular dynamics study—based on an implicit-solvent model for lipid bilayers—of the effect of solid substrates on the phase behavior of biomimetic membranes. The outcome of our study shows that the substrate leads to a non-symmetric transbilayer lipid distribution, with a lipid density of the proximal leaflet that is higher than that of the distal leaflet. The relative difference between the densities of the proximal and distal leaflets increases with increasing the strength of the attraction between the bilayer and the substrate.

Furthermore, we found that for relatively weak substrate-bilayer interactions, the order parameters of both proximal and distal leaflets exhibit an abrupt transition as a function of temperature, and these transitions occur at the same temperature. However, for strong substrate-bilayer interactions, while the order parameter of the proximal leaflet undergoes an abrupt change, the distal leaflet only exhibits a gradual increase with decreasing temperature. This is in qualitative agreement with the outcome of a recent experimental study by Ramkaram and Badia,[10] who also observed a more gradual increase in the gel fraction of the distal leaflet than in the proximal leaflet. A mean field theory based on the Bragg-Williams approximation predicts results that are in good qualitative agreement with our simulation results.

The main conclusion of our study is that the anomalous phase behavior of supported lipid bilayers is due to the following: the strong attractive interaction between the substrate and the lipid head groups of the proximal leaflet causes a translocation of lipids from the distal to proximal leaflets, thereby causing a transbilayer imbalance in the lipid density. As a result of this, while the proximal leaflet undergoes an abrupt phase change, a relatively low lipid density of the distal leaflet prevents a complete gelation of the lipids, so that a fraction of the lipids in the fluid phase are still present even at low temperatures.

ACKNOWLEDGMENTS

The authors would like to thank Professor Sarah Keller, Professor Steven Boxer, Professor Luis Bagatolli, and Professor Jie Yang for useful discussions. This work was supported by a grant from the National Institute of General Medical Sciences of the National Institutes of Health (No. R15GM106326). All simulations were performed on computers of the High Performance Computing Facility at the University of Memphis. The snapshots in Fig. 1 were generated using VMD version 1.9.3.[64]

[1] B. Alberts, A. Johnson, J. Leiws, and M. Raff, *Molecular Biology of the Cell*, 5th ed. (Garland Science, 2007).
[2] M. Bloom, E. Evans, and O. G. Mouritsen, Q. Rev. Biophys. **24**, 293 (1991).
[3] O. G. Mouritsen, *Life as a Matter of Fat* (Springer, 2005).
[4] M. Benes, D. Billy, A. Benda, H. Speijer, M. Hof, and W. T. Hermens, Langmuir **20**, 10129 (2004).
[5] R. M. Weis, K. Balakrishnan, B. A. Smith, and H. M. McConnell, J. Biol. Chem. **257**, 6440 (1982).
[6] A. A. Brian and H. M. McConnell, Proc. Natl. Acad. Sci. U. S. A **81**, 6159 (1984).
[7] M. C. Blosser, A. R. Honerkamp-Smith, T. Han, M. Haataja, and S. L. Keller, Biophys. J. **109**, 2317 (2015).
[8] Y. F. Dufrêne, W. R. Barger, J. B. D. Freen, and G. U. Lee, Langmuir **13**, 4779 (1997).
[9] H. Zan, V. P. Zhdanov, and N.-J. Cho, Langmuir **30**, 10363 (2014).
[10] M. Ramkaran and A. Badia, J. Phys. Chem. B **118**, 9708 (2014).
[11] J. Mou, J. Yang, C. Huang, and Z. Shao, Biochemistry **33**, 4439 (1994).
[12] D. Keller, N. B. Larsen, I. M. Moller, and O. G. Mouritsen, Phys. Rev. Lett. **94**, 025701 (2005).
[13] A. Charrier and F. Thibaudau, Biophys. J. **89**, 1094 (2005).
[14] Y. Gerelli, L. Porcar, and G. Fragneto, Langmuir **28**, 15922 (2012).
[15] J. M. Cranes, V. Kiessling, and L. K. Tamm, Langmuir **21**, 1377 (2005).
[16] T. M. Bayerl and M. Bloom, Biophys. J. **58**, 357 (1990).
[17] S. J. Johnson, T. M. Bayerl, D. C. McDermott, G. W. Adam, A. R. Rennie, R. K. Thomas, and E. Sackmann, Biophys. J. **59**, 289 (1991).
[18] J. Kim, G. Kim, and P. S. Cremer, Langmuir **17**, 7255 (2001).
[19] C. Naumann, T. Brumm, and T. M. Bayerl, Biophys. J. **63**, 1314 (1992).
[20] J. Yang and J. Appleyard, J. Phys. Chem. B **104**, 8097 (2000).
[21] F. Tokumasu, A. J. Jin, and J. A. Dvorak, J. Electron Microsc. **51**, 1 (2002).
[22] Z. V. Leonenko, E. Finot, H. Ma, T. E. Dahms, and D. T. Cramb, Biophys. J. **86**, 3783 (2004).
[23] F. Yarrow, T. J. H. Vlugt, J. P. J. M. van der Eerden, and M. M. Snel, J. Cryst. Growth **275**, e1417 (2005).
[24] Z. V. Feng, T. A. Spurlin, and A. A. Gewirth, Biophys. J. **88**, 2154 (2005).
[25] S. Garcia-Manyes, G. Oncins, and F. Sanz, Biophys. J. **89**, 4261 (2005).
[26] C. Scomparin, M. Ferreira, T. Charitat, and B. Tinland, Eur. Phys. J. E **28**, 211 (2009).
[27] H. M. Seeger, G. Marino, A. Alessandrini, and P. Facci, Biophys. J. **97**, 1067 (2009).
[28] H. M. Seeger, A. Di Cerbo, A. Alessandrini, and P. Facci, J. Phys. Chem. B **114**, 8926 (2010).
[29] A. Alessandrini and P. Facci, Soft Matter **10**, 7145 (2014).
[30] L. K. Tamm and H. M. McConnell, Biophys. J. **47**, 1–5 (1985).
[31] R. Homan and H. J. Pnwnall, Biochim. Biophys. Acta, Biomembr. **938**, 155 (1988).
[32] G. Parisio, A. Ferrarini, and M. M. Sperotto, Int. J. Adv. Eng. Sci. Appl. Math. **8**, 134 (2016).
[33] M. M. Sperotto and A. Ferrarini, in *Springer Series in Biophysics*, edited by B. Martinac (Springer).
[34] D. Marquardt, F. A. Heberle, T. Miti, B. Eicher, E. London, J. Katsaras, and G. Pabst, Langmuir (published online).
[35] C. Xing and R. Faller, J. Chem. Phys. **131**, 175104 (2009).
[36] R. Merkel, E. Sackmann, and E. Evans, J. Phys. **50**, 1535 (1989).
[37] L. Zhang and S. Granick, J. Chem. Phys. **123**, 211104 (2005).

[38]M. A. Deverall, S. Garg, K. Ludtke, R. Jordan, J. Ruthe, and C. A. Naumann, Soft Matter **4**, 1899 (2008).
[39]M. Hetzer, S. Heinz, S. Grage, and T. M. Bayerl, Langmuir **14**, 982 (1998).
[40]R. Nachan and M. Hof, Biochim. Biophys. Acta. Biomembr. **1798**, 1377 (2010).
[41]M. Tarek, K. Tu, M. L. Klein, and D. J. Tobias, Biophys. J. **77**, 964 (1999).
[42]D. R. Heine, A. R. Rammohan, and J. Balarishnan, Mol. Simul. **33**, 391 (2007).
[43]C. Xing and R. Faller, J. Phys. Chem. B **112**, 7086 (2008).
[44]M. Roark and S. E. Feller, Langmuir **24**, 12469 (2008).
[45]M. I. Hoopes, M. Deserno, M. L. Longo, and R. Faller, J. Chem. Phys. **129**, 175102 (2008).
[46]C. Xing, O. H. S. Ollila, I. Vattulainen, and R. Faller, Soft Matter **5**, 3258 (2009).
[47]C. Xing and R. Faller, Soft Matter **5**, 4526 (2008).
[48]H. L. Wu, P. Y. Chen, C. L. Chi, H. K. Tsao, and Y. J. Sheng, Soft Matter **9**, 1919 (2013).
[49]A. Perstin and M. Grunze, Biointerphases **7**, 57 (2012).
[50]A. Lamberg and T. Taniguchi, J. Phys. Chem. **118**, 10643 (2014).
[51]K. Dimitrievski, R. Reimhult, B. Kasemo, and V. P. Zhdanov, Colloids Surf., B **39**, 77 (2004).
[52]S. Loverde, F. J. Solis, and M. Olvera de la Cruz, Phys. Rev. Lett. **98**, 237802 (2007).
[53]J. D. Revalee, M. Laradji, and P. B. Sunil Kumar, J. Chem. Phys. **128**, 035102 (2008).
[54]M. Laradji, P. B. Sunil Kumar, and E. J. Spangler, J. Phys. D: Appl. Phys. **49**, 293001 (2016).
[55]D. H. Kim and J. A. Frangos, Biophys. J. **95**, 620 (2008).
[56]G. S. Grest and K. Kremer, Phys. Rev. A **33**, 3628 (1986).
[57]N. Metropolis, A. W. Rosenbluth, M. N. Rosenbluth, A. H. Teller, and E. Teller, J. Chem. Phys. **21**, 1087 (1953).
[58]W. C. Swope, H. C. Andersen, P. H. Berens, and K. R. Wilson, J. Chem. Phys. **76**, 637 (1982).
[59]J. F. Nagle, J. Chem. Phys. **58**, 252 (1973).
[60]S. Doniach, J. Chem. Phys. **68**, 4912 (1978).
[61]O. G. Mouritsen, A. Boothroyd, R. Harris, N. Jan, T. Lookman, L. MacDonald, D. A. Pink, and M. J. Zuckermann, J. Chem. Phys. **79**, 2027 (1983).
[62]D. Marsh, Chem. Phys. Lipids **57**, 109 (1991).
[63]T. Schubert, E. Schneck, and M. Tanaka, J. Chem. Phys. **135**, 055105 (2011).
[64]W. Humphrey, A. Drake, and K. Schulten, J. Mol. Graphics **14**, 33 (1996).